JVI Accepts, published online ahead of print on 10 December 2014
J. Virol. doi:10.1128/JVI.01981-14

Genetic Analysis of the Localization of APOBEC3F to Human Immunodeficiency Virus Type 1 (HIV-1) Virion Cores

John P. Donahue[a], Rebecca T. Levinson[b], Jonathan H. Sheehan[c], Lorraine Sutton[a], Harry E. Taylor[e], Jens Meiler[d], Richard T. D'Aquila[e#], and Chisu Song[e#]

[a]Division of Infectious Diseases, Department of Medicine, Vanderbilt University School of Medicine, Nashville, Tennessee, USA

[b]Center for Human Genetics Research, Vanderbilt University School of Medicine, Nashville, TN 37232

[c]Center for Structural Biology and Department of Biochemistry, Vanderbilt University, Nashville, Tennessee, USA

[d]Center for Structural Biology, Institute for Chemical Biology, and Departments of Chemistry, Pharmacology, and Biomedical Informatics, Vanderbilt University, Nashville Tennessee, USA

[e]Division of Infectious Diseases and Northwestern HIV Translational Research Center, Department of Medicine, Northwestern University Feinberg School of Medicine, Chicago, Illinois, USA

Running Head: APOBEC3F and C Core Localization

21 #Address correspondence to: richard.daquila@northwestern.edu or

22 chisu.song@northwestern.edu

23 303 East Superior Street

24 Robert H. Lurie Medical Research Center, Room 9-159

25 Northwestern University Feinberg School of Medicine

26 Phone: 312-503-0303 (RTD) or 312-503-2669 (CS)

27 Fax (for both corresponding authors): 312-503-3668

28

29 Abstract: 198 words

30 Text: 4,924 words

31 **ABSTRACT**

32

33 Members of the APOBEC3 family of cytidine deaminases vary in proportion of virion-
34 incorporated enzyme that is localized to mature retrovirus cores. We reported previously
35 that APOBEC3F (A3F) was highly localized into mature human immunodeficiency virus type
36 1 (HIV-1) cores and identified that L306 in the C-terminal cytidine deaminase (CD) domain
37 contributed to its core localization. We have now determined additional genetic
38 determinant(s) for A3F localization to HIV-1 cores. We found that one pair of leucines in
39 each of A3F's C-terminal and N-terminal CD domains jointly determined the degree of
40 localization of A3F into HIV-1 virion cores. These are A3F L306 / L368 (C-terminal domain)
41 and A3F L122 / L184 (N-terminal domain). Substitutions in one of these specific leucine
42 residues in either of the two A3F CD domains (A3F L368A; L122A; L184A) decreased core
43 localization and diminished HIV restriction, without changing virion packaging.
44 Furthermore, double mutants in these leucine residues in each of A3F's two CD domains
45 (A3F L368A plus L184A, or A3F L368A plus L122A) were still packaged into virions, but
46 completely lost core localization and anti-HIV activity. HIV virion core localization of A3F is
47 genetically separable from its virion packaging, and anti-HIV activity requires some core
48 localization.

49 Importance: Specific leucine-leucine interactions are identified as necessary for A3F's core
50 localization and anti-HIV activity, but not for its packaging into virions. Understanding these
51 signals may lead to novel strategies to enhance core localization that may augment effects of
52 A3F against HIV, and perhaps of other A3s against retroviruses, parvoviruses, and hepatitis
53 B virus.

54

55 **INTRODUCTION**

56

57 The members of Apolipoprotein B mRNA-editing enzyme catalytic, polypeptide-like
58 (APOBEC3 or A3) family of cytidine deaminases vary in several properties, and
59 understanding these biological differences will be critical to exploit their potential for
60 therapeutic use in humans. A3s differentially block replication of endogenous
61 retrotransposons (1-8), endogenous retroviruses (9-11), exogenous retroviruses (12-18),
62 adeno-associated virus (19, 20), as well as hepadnavirus (21-23). Family members also
63 differ in potency of virus restriction, deaminase target sequence specificity, relative
64 magnitude of cytidine deaminase-dependent antiviral activity, and their evasion of viral
65 countermeasures such as the virion infectivity factor (Vif) of human immunodeficiency
66 virus type 1 (HIV-1).

67 We recently reported that A3F and A3G, two family members that are relevant for
68 human restriction of HIV-1 replication, differed in their relative magnitude of localization to
69 virion cores (24). This is consistent with variation across the A3 family in the proportion of
70 virion-packaged enzyme localized to cores. Mouse APOBEC3 (mA3) was localized in the
71 cores of mouse mammary tumor virus and murine leukemia virus. It has antiviral activity
72 against those viruses (25-27). Increasing virion-incorporated mA3 also increased the
73 amount localized to cores (25). It has also been reported that human APOBEC3A (A3A) was
74 not localized to HIV-1 cores, and lacked HIV-1 restriction activity despite virion
75 incorporation; however, it gained antiviral activity when fused to another protein that
76 promoted its localization into virion cores (28, 29).

77 The current work focused on further characterizing genetic determinants of the
78 high degree of core localization of A3F (24), and studying whether the degree of A3F core

79 localization affects retroviral restriction. In addition, we tested the hypothesis that the
80 magnitude of A3F's localization into the mature viral core is not determined only by the
81 amount that is packaged into the virion (24, 25). This hypothesis was suggested by several
82 earlier results (24). Previously, we demonstrated that a chimeric A3F with its N-terminal CD
83 domain replaced by glutathione S-transferase (GST) maintained a similar level of
84 incorporation into HIV-1 virions as did the wild-type A3F, but exhibited decreases in both
85 core localization and HIV restriction (24). The data presented here identified specific amino
86 acid residues in A3F that play crucial roles for core localization and viral restriction without
87 changing packaging into retrovirus virions. Our results suggest that studying core
88 localization might help efforts to increase activities of A3F and other A3s against HIV, other
89 retroviruses, hepatitis B virus (HBV), and parvoviruses.

90

91 **MATERIALS AND METHODS**

92

93 **Cell Lines and Culture Conditions.** HEK293T cells were obtained from ATCC. TZM-bl cells
94 were obtained through the NIH AIDS Research and Reference Reagent Program from John C.
95 Kappes, Xiaoyun Wu, and Tranzyme, Inc. The TZM-bl indicator cell line, used for infectivity
96 assays, is a genetically engineered HeLa cell clone expressing CD4, CXCR4, CCR5, and Tat-
97 responsive firefly luciferase and *Escherichia coli* β-galactosidase under the control of an
98 HIV-1 long terminal repeat. HEK293T and TZM-bl cells were maintained in DMEM
99 (containing 4.5 g/liter glucose, L-glutamine, and sodium pyruvate) medium plus 10% fetal
100 bovine serum, 50 IU/ml penicillin, and 50 μg/ml streptomycin at 37 °C and 5% CO_2.

101

102 **Plasmids.** A pNL4.3 Vif-null mutant in which tandem nonsense mutations were introduced

103 in codons 26 and 27 of the Vif open reading frame was constructed by Ann Sheehy and
104 acquired with her permission from Una O'Doherty. The NL4.3 Vif-null clone was originally
105 derived from a full-length infectious HIV-1 clone, pNL4.3, and was isogenic with it except for
106 the nonsense mutations in Vif gene. A3F expression plasmid was constructed as described
107 before (24). The pcDNA3.1 HA-A3F expression plasmid was constructed by PCR
108 amplification of A3F sequences from pcDNA3.1 A3F using an A3F-specific forward primer
109 encoding the HA epitope with 5′-*Xba*I site and the vector-specific Bovine Growth Hormone
110 (BGH) reverse primer. Amplified HA-A3F DNA fragments were digested with *Xba*I and
111 *Hin*dIII and inserted in *Xba*I/*Hin*dIII digested pcDNA3.1(-). The resulting construct was
112 confirmed by DNA sequencing. A3C expression plasmid was obtained through the NIH AIDS
113 Research and Reference Reagent Program, Division of AIDS, NIAID, NIH deposited by Drs. B.
114 Matija Peterlin and Yong-Hui Zheng (30). The pcDNA3.1 HA-A3F/C-Tail expression plasmid
115 in which A3F C-terminal amino acid residues 348 to 373 were replaced with A3C C-terminal
116 residues 165 to 190 was constructed by ligating the C-terminal 488 bp A3C *Xba*I/*Bsr*GI
117 fragment with the N-terminal 1064 bp *Xba*I/*Bsr*GI fragment from pcDNA-HA-A3F in
118 pcDNA3.1 (-). Mutations were introduced into pcDNA-HA-A3F plasmid template using
119 appropriate mutagenic primers by a mega-primer PCR method as described previously
120 (31). Mutations were confirmed by DNA sequencing. The sequences of primers used for the
121 construction of all expression plasmids are available upon request.

122

123 **Antibodies.** The following antibody was obtained through the NIH AIDS Research and
124 Reference Reagent Program, Division of AIDS, NIAID, NIH: anti-APOBEC3F(C18) polyclonal
125 antibody which recognizes the C-terminal tail of A3F from Michael Malim (32). GAPDH and
126 anti-β-actin monoclonal antibody (clone AC-74) were from Sigma. Anti-HA rabbit polyclonal

127 antibody was from United States Biologicals. Anti-p24 monoclonal antibody 183-H12–5C
128 was from Vanderbilt-Meharry Center for AIDS Research Virology Core.

129

130 **Immunoblotting.** HEK293T cells were plated at a density of 6 × 10^5 cells/well in a 6-well
131 culture plate 24 h prior to transfection with 1 µg of pNL4.3 Vif-null and various amounts of
132 WT HA-A3F, HA-A3F-C tail or other A3F mutants, as indicated in individual figure legends.
133 Linear polyethylenimine (PEI; 25 kDa; Polysciences, Inc.) was used, as described (33).
134 Forty-eight hours after transfection, cells were lysed in 250 µl of cell lysis buffer (1X
135 Dulbecco's Phosphate-buffered Saline (Mediatech, Inc.), 1 mM Na_2EDTA, 0.5% Triton X-100
136 (v/v), and complete mini protease inhibitor mixture without Na_2EDTA (Roche) and
137 centrifuged at 10,000 × *g* for 5 min at 4 °C. Cell lysates were combined with an 25 µl of 2X
138 SDS-protein sample buffer (100 mM Tris-HCl, pH 6.8, 4 mM Na_2EDTA, 4% SDS, 4% 2-
139 mercaptoethanol, 20% glycerol, 0.1% bromphenol blue), heated at 100 °C for 5 min. and
140 analyzed by electrophoresis through a 12.5% SDS-polyacrylamide gel. After electrophoresis,
141 separated proteins were transferred to an Immobilon-P membrane (Millipore) and
142 processed for Western blot analysis using protein-specific antibodies with
143 chemiluminescent detection. Control experiments also evaluated if A3F-transfected
144 HEK293T cells secrete microvesicles containing A3F, and no evidence of this was identified.
145 Six million 293T cells were transiently transfected with 12 ug of A3F expression plasmids,
146 either wild type (WT) or mutants (A3F L122A, L184A, and L368A). Cell lysates and
147 supernatant fluids were collected 2 days after transfection. Supernatant fluids were
148 processed exactly as were those containing viral particles for sucrose density gradient
149 analyses (below). The resulting cell lysates and centrifuged supernatant fluids were
150 analyzed using immunoblotting, with blotting for GAPDH in cell lysates as a positive control.

151 No A3F immunoreactivity was detectable in the centrifuged supernatants despite abundant
152 cellular expression of each A3F and GAPDH (not shown). This is consistent with lack of
153 microvesicle secretion from HEK293T cells, as previously reported by others (34).

154

155 **Sucrose Density Gradient Centrifugation.** HEK293T cells were plated at a density of 6 ×
156 10^6 cells/100 mm culture dish 24 h prior to transfection. Cells were co-transfected with 15
157 μg of pNL4.3 Vif-null proviral clone and various amounts of A3 expression plasmid DNA, as
158 indicated in individual figure legends. Culture supernatants were collected 48 h after
159 transfection and cellular debris was removed by centrifugation or filtration through a 0.45
160 μm filter. HIV-1 particles were then concentrated by ultracentrifugation (100,000 X g for 3 h
161 at 4 °C) through a 20% sucrose cushion (w/v) in STE buffer (10 mM Tris-HCl, pH 7.4, 100
162 mM NaCl, 1 mM EDTA). Pelleted virions were resuspended in 300 μl of STE buffer, and
163 subjected to ultracentrifugation (130,000 X g for 16 h at 4 °C) through a layer of 1% Triton
164 X-100 into a linear 30–70% (w/v) sucrose density gradient, as described (35). After
165 centrifugation, 1 ml fractions were collected from the top of the gradient and stored at −20
166 °C. Specific proteins in individual fractions were analyzed by SDS-polyacrylamide gel
167 electrophoresis and immunoblotting. One-tenth milliliter (0.1 ml) of each fraction was
168 diluted with 0.1 ml STE buffer and the protein precipitated with an equal volume of 20%
169 trichloroacetic acid on ice for 30 min. The protein precipitate was washed twice with 0.3 ml
170 acetone, air dried, and dissolved in 25 μl of 2 X SDS-protein sample buffer. Samples were
171 heated at 100 °C for 5 min and 5 μl of each was fractionated by electrophoresis through a
172 12.5% SDS-polyacrylamide gel. After electrophoresis, separated proteins were transferred
173 to an Immobilon-P membrane and processed for Western blot analysis using protein-
174 specific antibodies with chemiluminescent detection.

175

176 **Viral Infectivity Assay.** TZM-bl indicator cells were plated at a density of 10,000 cells/well
177 in a 96 well culture plate 24 h prior to infection and incubated at 37 °C (5% CO_2). On the day
178 of infection, the culture medium was removed and the cells inoculated in triplicate with 100
179 µl of 2-fold serial dilutions of viral supernatants in culture medium containing 20 µg/ml
180 DEAE-dextran. After 24 hrs of incubation, culture medium was removed from each well and
181 replaced with 100 µl of Britelite Plus luciferase assay substrate (PerkinElmer). Following 5
182 min of incubation at room temperature, 75 µl of each cell lysate was transferred to a 96-well
183 OptiPlate 96 (PerkinElmer) and luminescence was measured in a VICTOR X2 Multilabel
184 Reader (PerkinElmer).

185

186 **Generation of A3F Structural Model.** An A3F model was built using Rosetta 3.3, a software
187 suite for predicting and designing protein structures, protein folding mechanisms, and
188 protein-protein interactions (36). The 1.38Å resolution structure of A3G, Protein Data Bank
189 (PDB) ID 3V4K (37), was used to build this model in order to gain more information about
190 amino acid side chains than present in the published structure of a modified A3F C-terminal
191 CD domain, PDB ID 4IOU (38). The sequence of the C-terminal domain of A3F used for
192 building the model (GenBank ID NP_660341.2 residues 193-373) differed from that of the
193 expression construct used in the biological experiments by a single amino acid, with the
194 expression construct containing an isoleucine and the computational model a valine residue
195 at amino acid 231. This difference was inadvertently introduced during cloning of the
196 expression construct. This A3F sequence was aligned to an edited sequence of the A chain of
197 3V4K from which irrelevant atoms such as ions and ligands had been removed. This
198 sequence alignment was used to thread the A3F sequence onto the A3G crystal structure. In

199 a two-step procedure, loop regions missing from the 3V4K structure were constructed, the
200 A3F model was relaxed, and A3F loops were then rebuilt to sample a larger conformational
201 space (36, 37, 39). 20,000 candidate models were generated initially. The top 2000 scoring
202 models were clustered by root-mean-square distance (RMSD) and ranked by Rosetta
203 energy score. The data and protocol used for Rosetta are detailed in a supplementary data
204 file (Supplemental Fig. 1). The best-scoring models of the ten largest clusters were selected
205 to represent the potential conformational diversity of the loops in A3F. All models were
206 visualized and figures were made using molecular visualization software (The PyMOL
207 Molecular Graphics System, Version 1.5.0.4 Schrödinger, LLC).

208

209 **RESULTS**

210

211 **Structural model of C-terminal CD domain of A3F indicated possible hydrophobic**
212 **interaction(s) between L306 and residues in α-helix 6 of the protein.** In a high
213 resolution crystal structure of a modified A3F C-terminal CD domain, PDB ID 4IOU (38), the
214 L306 side chain (Fig. 1A) previously identified as necessary, but not sufficient, for extensive
215 localization of A3F into the mature virion core (24) was close to the C-terminal α-helix 6
216 leucines at positions 364, and 368 (Fig. 1A). These leucines, and L372, in the A3F C-terminal
217 α-helix 6 each had their side chains oriented towards the interior of the protein (38).
218 However amino acid side chains were not fully built in the published model of the A3F
219 structure. Therefore, structural models of A3F were also built based on homology to the
220 highest resolution structure of a modified A3G C-terminal CD domain published to date,
221 which did build out side chains (PDBID 3V4K (37)), using Rosetta-3.3 (36). A model built on

222 homology to A3G compared well to the A3F crystal structure (38), and also supported the
223 hypothesis that L364 and L368 might have potential hydrophobic interaction with L306. In
224 each of the energy-minimized models of A3F structures derived from the A3G structure
225 (one representative structure of the top-scoring models is shown in Fig. 1B), the carbon
226 atoms of L306 and L368 were approximately 4 Å apart or less, a distance that could permit
227 hydrophobic interactions between L306 and L368 residues. The distances estimated
228 between L306 and L364 were slightly greater in our models. L372 was even more distant
229 from L306 in both the published A3F structure and the homology model based on the A3G
230 structure, suggesting that L372 lacked potential to interact with L306.

231

232 **Deletions of the α-helix 6 residues decrease core localization of A3F.** The amino acid
233 sequence of the C-terminal α-helix 6 starts at residue 358 in A3F (38, 40-42). By
234 introducing a stop codon in A3F at either amino acid 350 (HA-A3F 350) or 360 (HA-A3F
235 360), truncated mutants lacking all of the α-helix 6 region of A3F were constructed (Fig.
236 2A). The effect of each truncation mutant on viral core localization was then tested by co-
237 transfecting HEK293 cells with the Vif-null NL4.3 proviral clone and the truncation mutant
238 A3F expression plasmids. The resulting viral particles were concentrated and analyzed
239 using sucrose density gradients followed by immunoblotting (Fig.2B). Wild-type (WT) A3F
240 protein concentrated in gradient fractions corresponding to mature cores (fractions 9 and
241 10) (Fig. 2B HA-A3F WT). However, virion HA-A3F 350 and HA-A3F 360 proteins were
242 distributed across sucrose density gradient fractions more broadly than HA-A3F WT (Fig.
243 2B, second and third panels). The majority of both truncated mutant A3F proteins were
244 found in fractions 5 to 8, with a small amount in one core component-containing fraction.

245 The C-terminal α-helix 6 truncations altered more than the conserved leucines. We

246 assessed whether residues other than the C-terminal α-helix 6 leucines (at A3F residues
247 364, 368, and 372) affected core localization by using a chimeric A3F-A3C mutant protein.
248 A3C has the identical number of amino acid residues in its C-terminal α-helix 6 as does A3F.
249 However, only three of these amino acids are conserved between A3C and A3F; these are
250 the leucines corresponding to A3F L364, L368, and L372 (Fig. 2 A). Using a unique
251 restriction site, we constructed a chimera with the A3F residues starting at amino acid 348
252 replaced by the corresponding C-terminal 26 residues of A3C (HA-A3F/C Tail); the A3C
253 residues differ in every position other than the three leucines from the corresponding A3F
254 residues (Fig. 2A boxed region and 2C). Levels of cellular expression and viral incorporation
255 of HA-A3F/C Tail protein was equivalent to that of HA-A3F WT (data not shown). A sucrose
256 density gradient indicated that HA-A3F/C Tail was localized in mature virion cores as well
257 as HA-A3F WT (Fig. 2D). HA-A3F/C Tail also retained the same magnitude of antiviral
258 activity against Vif-null HIV-1 NL4.3 as wild-type A3F (data not shown). These results are
259 consistent with a role in core localization for one or more of the leucine residue(s) in α-
260 helix 6 of both A3C and A3F.

261

262 **Mutation of L368 in the A3F C-terminal α-helix 6 diminishes A3F's core localization**
263 **and its antiviral activity.** Since the results described above suggested that one or more of
264 the 3 conserved residues in the A3F C-terminal α-helix 6 (A3F L364, L368, L372; starred in
265 Fig. 2A) contribute to A3F's core localization, we introduced both single and double alanine
266 substitution mutations into each of them (Fig. 3A). The effects of these mutations on cellular
267 expression, viral incorporation, infectivity and core localization of A3F were tested as
268 described in Material and Methods.

269 Levels of cellular expression (Fig. 3B) and virion incorporation (Fig. 3C) of each of

270 the mutants with alanine replacing one of the α-helix 6 conserved leucine single mutants
271 (L364A, L368A and L372A, lanes 4, 5, and 6, respectively) were comparable to wild-type
272 A3F (lane 2). The single L306A mutant that was previously characterized (lane 3) had
273 slightly lower levels of cellular protein and viral incorporation, as seen before (24). In
274 addition, each of the double C-terminal leucine mutants (L364A/L368A, L368A/L372A, and
275 L306A/L368A, lanes 7, 8, and 9, respectively) also had a slight decrease in levels of cellular
276 protein (Fig. 3B) and virion incorporation (Fig. 3B and C). Of note, decreased cellular levels
277 and virion incorporation were previously shown not to alter the distinctive magnitude of
278 core localization of wild-type A3F versus A3G in sucrose density gradients (Fig. 1 and 2 in
279 (24)).

280 A3F L368A, which had comparable levels of cellular expression and viral
281 incorporation to the wild-type A3F, was found predominantly in gradient fractions 6 to 8;
282 only a small amount was present in one of the core component-containing fractions,
283 fraction 9 (Fig. 3D, third panel). This was similar to the lesser core localization of the A3F
284 L306A mutant (Fig. 3D, top panel, and Fig. 5B in (24)). In contrast, A3F mutants with either
285 L364A or L372A substitutions displayed a similar distribution across gradient fractions to
286 wild-type A3F; these two mutants each retained core localization similar to wild-type A3F
287 (Fig. 3D, second and fourth panels). Each of the double mutants tested that contained L368A
288 disrupted core localization (Fig. 3E). However, both L306/L368A and L364A/L368A
289 mutants had less protein localized to the mature core component containing fractions 9 and
290 10 than did the other double mutant (L368/L372) (Fig. 3E, second panel). These results
291 indicate that A3F L368 is the one of the three α-helix 6 conserved leucines that contributes
292 to core localization along with A3F L306.

293 Comparisons of infectivity of those mutants against Vif-null HIV-1 were made across

294 the three single α-helix 6 mutants (L364A, L368A, L372A) that had similar levels of virion
295 incorporation as wild-type A3F (gray bars in Fig. 3F), since decreased incorporation is itself
296 expected to diminish anti-HIV restriction activity. Infectivity was also compared across the
297 variants with similarly decreased expression and virion incorporation (L306A and each of
298 the 3 double mutants, white bars in Fig. 3F). HA-A3F L368A had decreased antiviral activity
299 against Vif-null HIV-1 compared to HA-A3F WT (Fig. 3F, row 5). In contrast, HA-A3F L364A
300 and HA-A3F L372A each displayed antiretroviral activity comparable to wild-type HA-A3F
301 (Fig. 3F, rows 2, 4 and 6). In contrast, antiviral activity was similarly decreased among the 4
302 variants with decreased incorporation (Fig. 3F, white bars). A3F L368A therefore is the only
303 of these mutants that had decreased anti-HIV activity along with decreased core localization
304 in the absence of any decrease in viral incorporation.

305

306 **Homologous residues in the N-terminal domain of A3F (L122 and L184) also**
307 **contribute to core localization and affect anti-viral activity against Vif-null HIV-1.**
308 Amino acid sequence alignment of N- and C-terminal CD domains of A3F indicated that the
309 C-terminal domain leucine residues critical for core localization were also conserved in the
310 N-terminus of A3F (Fig. 4A). Therefore, individual alanine substitution mutations were
311 introduced into these homologous residues in the A3F N-terminal CD domain (L122A,
312 L180A, L184A, and L188A) to test their effect on core localization into HIV-1 mature virion.
313 These were introduced through site-directed mutagenesis and mutations were confirmed
314 using DNA sequencing. 293T cells that were transiently transfected with the Vif-null HIV-1
315 NL4.3 clone and either HA-tagged WT or mutant A3Fs showed comparable cellular
316 expression of the single mutants (L122A, L180A, L184A and L188A) to that of wild-type
317 A3F (Fig. 4B) Each mutant protein was incorporated into viral particles similarly to WT (Fig.

318 4C). Sucrose density gradient analyses showed similar distribution across fractions for A3F
319 L180A and L188A as for WT A3F, with much of each mutant distributing in core
320 component-containing fractions (Fig. 4D, second and fourth panels). However, the majority
321 of HA-A3F L122A and L184A were found in fractions 4 to 8 with only a small amount in one
322 of the core component-containing fractions 9 and 10 (Fig. 4D, top and third panels). A3F
323 L180A and L188A had equivalent anti-viral activity against Vif-null HIV-1 to WT A3F, while
324 A3F L122A and L184A mutants each had reduced activity (Fig. 4E). Thus, L122A and L184A
325 in N-terminal domain of A3F also disrupted the extensive core localization and decreased
326 anti-viral restriction activity against Vif-null HIV-1. This corresponded to the effects of
327 mutating the homologous C-terminal residues, L306 and L368 of A3F.

328

329 **Disrupting the implicated leucine pairs in both N- and C-terminus CD domains**
330 **completely abrogates A3F's core localization and anti-viral activity against Vif-null**
331 **HIV-1.** Each of the mutants studied thus far that decreased core localization (A3F L122A,
332 L184A, L306A, and L368A) retained a single CD domain core localization signal, and were
333 distributed similarly in sucrose density gradient experiments to A3G (Figs. 1 and 2 in (24)).
334 In other words, some protein localized to core fractions, albeit less than for WT A3F. We
335 next tested whether mutating the two leucine pairs, one each in the N- and C-terminal CD
336 domain of A3F, and thereby affecting both domains, would more markedly affect core
337 localization. We constructed double mutants with one leucine in each CD domain changed
338 to alanine; the mutants were A3F L122A/L368A and L184A/L368A. (Since the cellular
339 expression level of the L306A mutant is lower than that of WT A3F, we did not include that
340 substitution in these double mutants.) The effects of the double mutants were tested on
341 cellular expression, viral incorporation, anti-viral activity and core localization as described

342 in Materials and Methods. The double mutants displayed similar levels of cellular
343 expression and viral incorporation to wild-type A3F (Fig. 5A, B). However, both A3F
344 L122A/L368A and L184A/L368A mutants were localized completely outside mature cores
345 (Fig. 5C) with no appreciable anti-viral activity against Vif-null HIV-1 (Fig. 5D).

346

347 **DISCUSSION**

348

349 A pair of leucines in each A3F CD domain is identified here as necessary for core
350 localization: L368 together with the previously described L306 in the C-terminal CD domain
351 and L122 with L184 in the N-terminal CD domain. This extends our previous report that a
352 greater proportion of virion-incorporated A3F than A3G co-localized with components of
353 the mature virion core in linear sucrose density gradients following mild detergent
354 treatment. Subsequently, others confirmed greater core localization of A3F than A3G using
355 imaging of fluorescent-tagged fusion proteins (43), validating results of the density gradient
356 methodology used here with an independent experimental approach. Our earlier results
357 also identified that A3F had two core localization signals (24). The current results add
358 further evidence that signals in each of A3F's two CD domains work together to increase
359 localization into HIV-1 viral mature core. Substituting an alanine for one of the leucines in a
360 single pair in one A3F domain decreased its core localization and restriction of Vif-null HIV-
361 1. In contrast, substituting an alanine for a leucine in both of these leucine pairs in each
362 domain completely abrogated A3F's core localization and restriction, even when virion
363 incorporation itself was not affected. Further, these results indicate that core localization is
364 genetically separable from virion packaging, as suggested by several earlier results (24, 44),
365 and that core localization may contribute to anti-HIV activity of A3F.

366 Structural modeling suggested that two leucines in the C-terminal domain α-helix 6
367 region of A3F (L364 and L368) were in close enough proximity for hydrophobic interaction
368 within the interior of the protein with L306, which was previously characterized as
369 contributing to A3F core localization. A3F mutants with truncations of the C-terminal α-
370 helix 6 did not localize to cores, consistent with a role for the α-helix 6. To exclude the
371 possibility that residues other than the leucines in α-helix 6 contributed to core localization,
372 we studied a chimeric protein in which the C-terminal α-helix 6 of A3F was replaced with
373 the homologous region from A3C. The leucines corresponding to A3F L364, L368, and L372
374 were the only residues unchanged from those in A3F in this chimeric protein. The finding
375 that this chimera was localized to cores similarly to A3F led to mutagenesis of each of the 3
376 leucine residues (364, 368, and 372). A3F L368A in the C-terminal deaminase domain
377 decreased core localization; no change was seen with mutagenesis of either of the other two
378 conserved leucines in α-helix 6, A3F L364A or L372A. This confirmed that L306 and L368
379 were both necessary for core localization.

380 These two leucines in the C-terminal domain, L306 and L368, of A3F are in close
381 enough proximity for hydrophobic interaction with each other in the published A3F C-
382 terminal domain crystal structure (38). An additional model was developed here by
383 homology to a high resolution structure of the A3G C-terminal domain (37, 41) in order to
384 add more amino side chain information than was present in the solved A3F crystal
385 structure. This also supported that A3F L368 was close enough to A3F L306 for
386 hydrophobic or van der Waals interactions. The other A3F C-terminal α-helix 6 leucines,
387 A3F L364 and A3F L372, were more distant from A3F L306 in both models.

388 The A3F C-terminal domain structure positions the L306/L368 leucine pair within
389 the protein's interior (38). Therefore, we speculate that this leucine pair, along with the

390 homologous pair in the N-terminal domain, may affect protein folding rather than mediating
391 an interaction on the surface of the protein with a virion component that causes core
392 localization. Indeed, the slightly decreased levels of cellular expression and virion
393 incorporation of A3F L306A noted earlier (24) could be consistent with A3F L306A having
394 deleterious effects on protein folding. However, all the other three single mutations (L368A,
395 L122A, and L184A) in the implicated leucine residues of A3F did not cause any decrease in
396 levels of cellular expression or virion incorporation detected by immunoblotting. This does
397 not completely exclude possible effects of these other mutants on protein folding. However,
398 these results do indicate that core localization of A3F can be diminished in the absence of
399 detectable decreases in its viral incorporation.

400 Determination of the mechanism whereby a leucine pair in each of two domains
401 leads to a greater degree of virion core localization of A3F will require analyses that are
402 beyond the scope of this report. Leucine-pair optimized folding of two domains, rather than
403 one, may lead to twice as much interaction with a virion component that facilitates core
404 localization. Alternatively, leucine pair-optimized folding of each domain may be needed for
405 the correct conformation of a two-domain monomer (or oligomer) of A3F that improves a
406 single interaction with an as-yet unidentified virion component. We hypothesize that core
407 localization requires binding to only a subset (or one) of multiple virion components that
408 mediate virion packaging. This may help explain why some A3 mutations affect both virion
409 packaging and core localization, while others affect only one of these processes.

410 It is also worth noting that earlier work showed that A3F W126A decreases
411 localization into HIV cores, in addition to impairing interaction with nucleocapsid and HIV-1
412 virion incorporation (24, 45). Decreased HIV virion incorporation of A3F W126A was
413 associated with decreased binding to 7SL RNA, and no decrement of binding to HIV genomic

414 RNA or 5s rRNA was found (45). RNase digestion of detergent-treated viral particles
415 containing A3F (either WT, L122A, L184A, or L368A) prior to density gradient
416 centrifugation was done as an initial test of the hypothesis that A3F core localization
417 involves interaction with a virion RNA. However, RNase digestion did not alter the
418 distribution of each A3F in the gradient (data not shown). This does not support that
419 hypothesis, although interaction with a RNA not accessible to RNase digestion cannot be
420 excluded.

421 A3F mutations that specifically decreased localization to HIV cores diminished its
422 anti-HIV restriction activity. This could be due to decreased virion core association itself, or
423 to changes in protein structure that independently affect both core association and
424 restriction activity. Core localization of mA3 has been shown to be important for its
425 deaminase-independent activity against MMTV and MLV (25-27, 46), and for anti-HIV
426 activity of A3A (28, 29). The magnitude of loss of anti-viral activity against Vif-null HIV-1 for
427 each of the A3F mutants that had decreased core localization (A3F L122A, L184A L306A,
428 L368A, L364A/L368A, L368A/L372A and L306A/L368A) was similar to that of the
429 deaminase-defective A3F E251Q, which did not have any alteration in core localization
430 compared to wild-type A3F (data not shown). Thus, these experiments suggest the
431 possibility that a similar diminishment in restriction activity occurs when A3F either loses
432 its intrinsic deaminase activity or its access to the HIV genome in the core that is the target
433 for deamination. However, intrinsic differences between different A3s (e.g.; A3F versus
434 A3G) may be more important in determining relative antiviral potency of the different
435 enzymes than relative magnitude of core localization. It has been shown that A3F's
436 deaminase activity is intrinsically limited relative to that of A3G (47) and the more core-
437 associated A3F may not be more potent in restricting HIV than is A3G (24, 32, 48).

438 Further study of mechanisms underlying the relatively better core localization of
439 A3F may lead to the potential for "virion engineering" to therapeutically maximize antiviral
440 effects of other A3s in the future. For example, small molecules might be developed that
441 could stabilize a conformation that increases A3G's limited localization into cores, which
442 may increase its overall anti-HIV activity and decrease the potential for evasion of Vif via
443 decreased virion incorporation (49, 50). Since the residues of A3F and A3G to which HIV-1
444 Vif binds to facilitate their proteasomal degradation are distinct from core-localizing
445 determinants, agents being developed to antagonize Vif may not decrease core localization
446 that enhances anti-viral activity against Vif-null HIV by A3F. Since core localization is
447 implicated in anti-parvovirus activities of A3 enzymes (19, 20), and at least a portion of
448 their anti-HBV activity (22, 51-55), increased basic understanding of core localization also
449 holds promise for improved treatments for those viruses.

450

451 **ACKNOWLEDGEMENTS**

452 The authors thank the NIH AIDS Reference and Reagent Program, Division of AIDS, NIAID
453 which provided plasmids, antibodies and cell line. Grant support was provided by R01
454 AI29193 and T32 GM080178. The D'Aquila laboratory also acknowledges support from the
455 Northwestern Medicine Catalyst Fund. Work in the Meiler laboratory is supported through
456 NIH (R01 GM080403, R01 MH090192, R01 GM099842, R01 DK097376) and NSF (Career
457 0742762).

458

459 **REFERENCES**

460

461 1. **Bogerd HP, Wiegand HL, Hulme AE, Garcia-Perez JL, O'Shea KS, Moran JV,**
462 **Cullen BR.** 2006. Cellular inhibitors of long interspersed element 1 and Alu
463 retrotransposition. Proc. Natl. Acad. Sci. U. S. A. **103:**8780-8785.

464 2. **Chiu YL, Witkowska HE, Hall SC, Santiago M, Soros VB, Esnault C, Heidmann T,**
465 **Greene WC.** 2006. High-molecular-mass APOBEC3G complexes restrict Alu
466 retrotransposition. Proc. Natl. Acad. Sci. U. S. A. **103:**15588-15593.

467 3. **Dutko JA, Schafer A, Kenny AE, Cullen BR, Curcio MJ.** 2005. Inhibition of a yeast
468 LTR retrotransposon by human APOBEC3 cytidine deaminases. Curr. Biol. **15:**661-
469 666.

470 4. **Esnault C, Millet J, Schwartz O, Heidmann T.** 2006. Dual inhibitory effects of
471 APOBEC family proteins on retrotransposition of mammalian endogenous
472 retroviruses. Nucleic Acids Res. **34:**1522-1531.

473 5. **Muckenfuss H, Hamdorf M, Held U, Perkovic M, Lower J, Cichutek K, Flory E,**
474 **Schumann GG, Munk C.** 2006. APOBEC3 proteins inhibit human LINE-1
475 retrotransposition. J. Biol. Chem. **281:**22161-22172.

476 6. **Schumacher AJ, Hache G, Macduff DA, Brown WL, Harris RS.** 2008. The DNA
477 deaminase activity of human APOBEC3G is required for Ty1, MusD, and human
478 immunodeficiency virus type 1 restriction. J. Virol. **82:**2652-2660.

479 7. **Schumacher AJ, Nissley DV, Harris RS.** 2005. APOBEC3G hypermutates genomic
480 DNA and inhibits Ty1 retrotransposition in yeast. Proc. Natl. Acad. Sci. U. S. A.
481 **102:**9854-9859.

482 8. **Stenglein MD, Harris RS.** 2006. APOBEC3B and APOBEC3F inhibit L1
483 retrotransposition by a DNA deamination-independent mechanism. J. Biol. Chem.
484 **281:**16837-16841.

485 9. **Armitage AE, Katzourakis A, de Oliveira T, Welch JJ, Belshaw R, Bishop KN,**
486 **Kramer B, McMichael AJ, Rambaut A, Iversen AK.** 2008. Conserved footprints of
487 APOBEC3G on Hypermutated human immunodeficiency virus type 1 and human
488 endogenous retrovirus HERV-K(HML2) sequences. J. Virol. **82:**8743-8761.

489 10. **Esnault C, Heidmann O, Delebecque F, Dewannieux M, Ribet D, Hance AJ,**
490 **Heidmann T, Schwartz O.** 2005. APOBEC3G cytidine deaminase inhibits
491 retrotransposition of endogenous retroviruses. Nature **433:**430-433.

492 11. **Lee YN, Malim MH, Bieniasz PD.** 2008. Hypermutation of an ancient human
493 retrovirus by APOBEC3G. J. Virol. **82:**8762-8770.

494 12. **Delebecque F, Suspene R, Calattini S, Casartelli N, Saib A, Froment A, Wain-**
495 **Hobson S, Gessain A, Vartanian JP, Schwartz O.** 2006. Restriction of foamy viruses
496 by APOBEC cytidine deaminases. J. Virol. **80:**605-614.

497 13. **Jonsson SR, LaRue RS, Stenglein MD, Fahrenkrug SC, Andresdottir V, Harris RS.**
498 2007. The restriction of zoonotic PERV transmission by human APOBEC3G. PLoS
499 One **2:**e893.

500 14. **Mangeat B, Turelli P, Caron G, Friedli M, Perrin L, Trono D.** 2003. Broad
501 antiretroviral defence by human APOBEC3G through lethal editing of nascent
502 reverse transcripts. Nature **424:**99-103.

503 15. **Takeda E, Tsuji-Kawahara S, Sakamoto M, Langlois MA, Neuberger MS, Rada C,**
504 **Miyazawa M.** 2008. Mouse APOBEC3 restricts friend leukemia virus infection and
505 pathogenesis in vivo. J. Virol. **82:**10998-11008.

506 16. **Low A, Okeoma CM, Lovsin N, de las Heras M, Taylor TH, Peterlin BM, Ross SR,**
507 **Fan H.** 2009. Enhanced replication and pathogenesis of Moloney murine leukemia
508 virus in mice defective in the murine APOBEC3 gene. Virology **385:**455-463.

509 17. **Okeoma CM, Low A, Bailis W, Fan HY, Peterlin BM, Ross SR.** 2009. Induction of
510 APOBEC3 in vivo causes increased restriction of retrovirus infection. J. Virol.
511 **83:**3486-3495.

512 18. **Okeoma CM, Petersen J, Ross SR.** 2009. Expression of murine APOBEC3 alleles in
513 different mouse strains and their effect on mouse mammary tumor virus infection. J.
514 Virol. **83:**3029-3038.

515 19. **Chen H, Lilley CE, Yu Q, Lee DV, Chou J, Narvaiza I, Landau NR, Weitzman MD.**
516 2006. APOBEC3A is a potent inhibitor of adeno-associated virus and
517 retrotransposons. Curr. Biol. **16:**480-485.

518 20. **Narvaiza I, Linfesty DC, Greener BN, Hakata Y, Pintel DJ, Logue E, Landau NR,**
519 **Weitzman MD.** 2009. Deaminase-independent inhibition of parvoviruses by the
520 APOBEC3A cytidine deaminase. PLoS Pathog. **5:**e1000439.

521 21. **Baumert TF, Rosler C, Malim MH, von Weizsacker F.** 2007. Hepatitis B virus DNA
522 is subject to extensive editing by the human deaminase APOBEC3C. Hepatology
523 **46:**682-689.

524 22. **Rosler C, Kock J, Kann M, Malim MH, Blum HE, Baumert TF, von Weizsacker F.**
525 2005. APOBEC-mediated interference with hepadnavirus production. Hepatology
526 **42:**301-309.

527 23. **Suspene R, Guetard D, Henry M, Sommer P, Wain-Hobson S, Vartanian JP.** 2005.
528 Extensive editing of both hepatitis B virus DNA strands by APOBEC3 cytidine
529 deaminases in vitro and in vivo. Proc. Natl. Acad. Sci. U. S. A. **102:**8321-8326.

530 24. **Song C, Sutton L, Johnson M, D'Aquila R, Donahue J.** 2012. Signals in APOBEC3F
531 N-terminal and C-terminal deaminase domains each contribute to encapsidation in
532 HIV-1 virions and are both required for HIV-1 restriction. The Journal of biological
533 chemistry **287:**16965-16974.

534 25. **MacMillan AL, Kohli RM, Ross SR.** 2013. APOBEC3 inhibition of mouse mammary
535 tumor virus infection: the role of cytidine deamination versus inhibition of reverse
536 transcription. J. Virol. **87:**4808-4817.

537 26. **Rulli SJ, Jr., Mirro J, Hill SA, Lloyd P, Gorelick RJ, Coffin JM, Derse D, Rein A.**
538 2008. Interactions of murine APOBEC3 and human APOBEC3G with murine
539 leukemia viruses. J. Virol. **82:**6566-6575.

540 27. **Zhang L, Li X, Ma J, Yu L, Jiang J, Cen S.** 2008. The incorporation of APOBEC3
541 proteins into murine leukemia viruses. Virology **378:**69-78.

542 28. **Aguiar RS, Lovsin N, Tanuri A, Peterlin BM.** 2008. Vpr.A3A chimera inhibits HIV
543 replication. J. Biol. Chem. **283:**2518-2525.

544 29. **Goila-Gaur R, Khan M, Miyagi E, Kao S, Strebel K.** 2007. Targeting APOBEC3A to
545 the viral nucleoprotein complex confers antiviral activity. Retrovirology **4:**61.

546 30. **Zheng YH, Irwin D, Kurosu T, Tokunaga K, Sata T, Peterlin BM.** 2004. Human
547 APOBEC3F is another host factor that blocks human immunodeficiency virus type 1
548 replication. J. Virol. **78:**6073-6076.

549 31. **Song C, Dubay SR, Hunter E.** 2003. A tyrosine motif in the cytoplasmic domain of
550 mason-pfizer monkey virus is essential for the incorporation of glycoprotein into
551 virions. J. Virol. **77:**5192-5200.

552 32. **Holmes RK, Koning FA, Bishop KN, Malim MH.** 2007. APOBEC3F can inhibit the
553 accumulation of HIV-1 reverse transcription products in the absence of
554 hypermutation. Comparisons with APOBEC3G. J. Biol. Chem. **282:**2587-2595.

555 33. **Durocher Y, Perret S, Kamen A.** 2002. High-level and high-throughput
556 recombinant protein production by transient transfection of suspension-growing
557 human 293-EBNA1 cells. Nucleic Acids Res. **30:**E9.

558 34. **Taylor HE, Khatua AK, Popik W.** 2014. The innate immune factor apolipoprotein
559 L1 restricts HIV-1 infection. J. Virol. **88:**592-603.

560 35. **Kotov A, Zhou J, Flicker P, Aiken C.** 1999. Association of Nef with the human
561 immunodeficiency virus type 1 core. J. Virol. **73:**8824-8830.

562 36. **Leaver-Fay A, Tyka M, Lewis SM, Lange OF, Thompson J, Jacak R, Kaufman K,**
563 **Renfrew PD, Smith CA, Sheffler W, Davis IW, Cooper S, Treuille A, Mandell DJ,**
564 **Richter F, Ban YE, Fleishman SJ, Corn JE, Kim DE, Lyskov S, Berrondo M,**
565 **Mentzer S, Popovic Z, Havranek JJ, Karanicolas J, Das R, Meiler J, Kortemme T,**
566 **Gray JJ, Kuhlman B, Baker D, Bradley P.** 2011. ROSETTA3: an object-oriented
567 software suite for the simulation and design of macromolecules. Methods Enzymol.
568 **487:**545-574.

569 37. **Li M, Shandilya SM, Carpenter MA, Rathore A, Brown WL, Perkins AL, Harki DA,**
570 **Solberg J, Hook DJ, Pandey KK, Parniak MA, Johnson JR, Krogan NJ,**
571 **Somasundaran M, Ali A, Schiffer CA, Harris RS.** 2012. First-in-class small
572 molecule inhibitors of the single-strand DNA cytosine deaminase APOBEC3G. ACS
573 Chem. Biol. **7:**506-517.

574 38. **Bohn M-F, Shandilya S, Albin J, Kouno T, Anderson B, McDougle R, Carpenter M,**
575 **Rathore A, Evans L, Davis A, Zhang J, Lu Y, Somasundaran M, Matsuo H, Harris**
576 **R, Schiffer C.** 2013. Crystal Structure of the DNA Cytosine Deaminase APOBEC3F:
577 The Catalytically Active and HIV-1 Vif-Binding Domain. Structure (London, England :
578 1993).

579 39. **Combs SA, Deluca SL, Deluca SH, Lemmon GH, Nannemann DP, Nguyen ED,**
580 **Willis JR, Sheehan JH, Meiler J.** 2013. Small-molecule ligand docking into
581 comparative models with Rosetta. Nat. Protoc. **8:**1277-1298.

582 40. **Shandilya SM, Nalam MN, Nalivaika EA, Gross PJ, Valesano JC, Shindo K, Li M,**
583 **Munson M, Royer WE, Harjes E, Kono T, Matsuo H, Harris RS, Somasundaran M,**
584 **Schiffer CA.** 2010. Crystal structure of the APOBEC3G catalytic domain reveals
585 potential oligomerization interfaces. Structure **18:**28-38.

586 41. **Shlyakhtenko L, Lushnikov A, Miyagi A, Li M, Harris R, Lyubchenko Y.** 2012.
587 Nanoscale structure and dynamics of ABOBEC3G complexes with single-stranded
588 DNA. Biochemistry **51:**6432-6440.

589 42. **Chen KM, Harjes E, Gross PJ, Fahmy A, Lu Y, Shindo K, Harris RS, Matsuo H.**
590 2008. Structure of the DNA deaminase domain of the HIV-1 restriction factor
591 APOBEC3G. Nature **452:**116-119.

592 43. **Burdick RC, Hu WS, Pathak VK.** 2013. Nuclear import of APOBEC3F-labeled HIV-1
593 preintegration complexes. Proc. Natl. Acad. Sci. U. S. A. **110:**E4780-4789.

594 44. **Hache G, Liddament MT, Harris RS.** 2005. The retroviral hypermutation specificity
595 of APOBEC3F and APOBEC3G is governed by the C-terminal DNA cytosine
596 deaminase domain. J. Biol. Chem. **280:**10920-10924.

597 45. **Wang T, Tian C, Zhang W, Sarkis PT, Yu XF.** 2008. Interaction with 7SL RNA but
598 not with HIV-1 genomic RNA or P bodies is required for APOBEC3F virion
599 packaging. J. Mol. Biol. **375:**1098-1112.

600 46. **Sanchez-Martinez S, Aloia AL, Harvin D, Mirro J, Gorelick RJ, Jern P, Coffin JM,**
601 **Rein A.** 2012. Studies on the restriction of murine leukemia viruses by mouse
602 APOBEC3. PLoS One **7:**e38190.

603 47. **Ara A, Love RP, Chelico L.** 2014. Different mutagenic potential of HIV-1 restriction
604 factors APOBEC3G and APOBEC3F is determined by distinct single-stranded DNA
605 scanning mechanisms. PLoS Pathog. **10:**e1004024.

606 48. **Zennou V, Bieniasz PD.** 2006. Comparative analysis of the antiretroviral activity of
607 APOBEC3G and APOBEC3F from primates. Virology **349:**31-40.

608 49. **Haché G, Shindo K, Albin J, Harris R.** 2008. Evolution of HIV-1 isolates that use a
609 novel Vif-independent mechanism to resist restriction by human APOBEC3G.
610 Current biology : CB **18:**819-824.

611 50. **Hache G, Abbink TE, Berkhout B, Harris RS.** 2009. Optimal translation initiation
612 enables Vif-deficient human immunodeficiency virus type 1 to escape restriction by
613 APOBEC3G. J. Virol. **83:**5956-5960.

614 51. **Nguyen DH, Gummuluru S, Hu J.** 2007. Deamination-independent inhibition of
615 hepatitis B virus reverse transcription by APOBEC3G. J. Virol. **81:**4465-4472.

616 52. **Li D, Liu J, Kang F, Guan W, Gao X, Wang Y, Sun D.** 2011. Core-APOBEC3C
617 chimerical protein inhibits hepatitis B virus replication. J. Biochem. **150:**371-374.

618 53. **Turelli P, Mangeat B, Jost S, Vianin S, Trono D.** 2004. Inhibition of hepatitis B
619 virus replication by APOBEC3G. Science **303:**1829.

620 54. **Rosler C, Kock J, Malim MH, Blum HE, von Weizsacker F.** 2004. Comment on
621 "Inhibition of hepatitis B virus replication by APOBEC3G". Science **305:**1403; author
622 reply 1403.

623 55. **Noguchi C, Hiraga N, Mori N, Tsuge M, Imamura M, Takahashi S, Fujimoto Y,**
624 **Ochi H, Abe H, Maekawa T, Yatsuji H, Shirakawa K, Takaori-Kondo A, Chayama**
625 **K.** 2007. Dual effect of APOBEC3G on Hepatitis B virus. J. Gen. Virol. **88:**432-440.

626

627

628 **FIGURE LEGENDS**

629

630 **FIG. 1.** A3F structural models are consistent with L306 interacting with L368. (A) The
631 structure of the entire modified A3F C-terminal CD domain (PDB ID 4IOU) (38), resolved to
632 2.75 Å, is depicted. (B) The relevant C-terminal region is magnified from the published
633 determination of the structure of the A3F C-terminal CD domain (PDB ID 4IOU) (38). The α-
634 helix 6 is on the bottom, with the C-terminus of the protein to the left. The DNA substrate
635 recognition loop between β-sheet 4 and α-helix 4 is on the top and includes L306, which is

636 oriented downwards. L368 in α-helix 6 is to the left of L306 and oriented upward. L364 in
637 α-helix 6 is to the right of L306 and oriented upward. L306 is closer to L368 than L364. The
638 amino acid side chains are not fully built in this model, as deposited in PDB. The wire mesh-
639 like overlay is a representation of the volume of the amino acid side chains in the model. (C)
640 The same potential interaction was seen in different models of A3F based on homology to
641 the better-resolved (1.38 Å) structure of a modified A3G C-terminal CD domain (PDB ID
642 3V4K) (37). One representative homology model of A3F from among the best-scoring
643 models (using Rosetta-3.3) (36) is depicted. The wire mesh-like overlay is a representation
644 of the volume of the amino acid side chains in the model. α-helix 6 is on the bottom, with the
645 C-terminus of the protein to the left of the figure. The DNA substrate recognition loop
646 between β-sheet 4 and α-helix 4 is on the top of the figure and includes L306, which is
647 oriented downwards. L368 in α-helix 6 is to the left of L306, and oriented upward. L364 in
648 α-helix 6 is to the right of L306, and oriented upward. Distances are less than 4 Å, and
649 estimated to allow hydrophobic interactions between the hydrogen atoms of L306 and
650 L368; distances are slightly greater between atoms of L306 and L364. L372 is not shown, as
651 it is one residue before the C terminus and too distant to potentially interact with L306.
652 There were 18 additional amino acids at the N-terminus of the A3F whose structure was
653 experimentally determined (38), relative to the A3F sequence used for building models
654 based on homology to A3G here. Among the residues in common between A3F used here
655 and in (38), 93.9% of the amino acids were identical. There were differences, however, in
656 three of the nine amino acids in the DNA substrate recognition loop from residues 307 to
657 315 (the loop between β-strand 4 and α-helix 4). The published crystal structures of A3G
658 (37) and A3F (38) also differed markedly in number, sequence and orientation of the amino
659 acid backbone of the DNA substrate recognition loop from residue 307 to 315, although
660 L306 was positioned very similarly in the published crystal structures of A3G (37) and A3F

661 (38). The amino acid backbone structure of the A3F homology model determined here
662 differed from that of PDB ID 4IOU by an overall RMSD of 3.2 Å, with a smaller difference
663 between them specifically in α-helix 6 (RMSD of 1.5 Å), validating the homology-based
664 model.

665

666 **FIG. 2.** Truncation mutations in C-terminal domain of A3F decrease core localization of A3F
667 while A3F/A3C C-terminus chimeras maintain core localization, suggesting that conserved
668 α-helix 6 leucine residues play a role in mature core localization of A3F. In these
669 experiments 10 μg of pNL4.3 Vif-null proviral clone and or 3 μg of each mutant A3F
670 expression DNAs were used for transient transfection. After 2 days post transfection cell
671 lysates and viral supernatants were collected to test its effect on core localization of the
672 mutant A3Fs. (A) Sequence alignment of the C-terminal α-helix 6 of C-terminal residues of
673 A3F and A3C. Only 3 leucines are conserved between A3F and A3C (starred) in α-helix 6
674 starting at amino acids 358 of A3F. DNA encoding the boxed residues of A3C (amino acids
675 165 to 190) replaced the boxed residues of A3F-C (amino acids 348 to 373) in the HA-
676 A3F/C Tail construct. Residues 350 and 360 are also depicted where termination of A3F
677 truncation mutants were engineered (respectively, HA-A3F 350 and HA-A3F 360). (B)
678 Sucrose density gradient centrifugation followed by imunoblotting using specific antibodies
679 and chemiluminescent detection compared mutants to HA-A3F-WT (top panel). HA-A3F
680 350 (second panel) and HA-A3F 360 (third panel) lost quantitative encapsidation. (C)
681 Schematic representations of wild-type A3F and A3F/A3C chimeric fusion protein (HA-
682 A3F/C-Tail) show relative locations of zinc-binding cytidine deaminase active site motifs in
683 white and other A3F coding sequences in grey. Hatches indicate A3C residues (A3C amino
684 acids 165 to 190) in C-terminal α-helix 6 that replaced the A3F residues 348 to 373 in HA-

685 A3F/C-Tail. (D) HA-A3F/C-Tail (second panel) had mature core localization similar to HA-
686 A3F-WT (first panel), with much of the A3 in fractions 9 and 10 that also contain mature
687 core-localized capsid ($p24^{Gag}$).

688

689 **FIG. 3.** Mutageneses confirm that interaction between A3F L368 and L306 is critical for
690 quantitative encapsidation of A3F. In these experiments 10 μg of pNL4.3 Vif-null proviral
691 clone and 1 μg of wild type or 3 μg of each mutant A3F expression DNAs were used for
692 transient transfection. After 2 days post transfection cell lysates and viral supernatants
693 were collected to test its effect on cellular expression, viral incorporation, infectivity and
694 core localization of the mutant A3Fs. (A) Alanine scanning mutations introduced into
695 conserved leucines of A3F are diagrammed. (B) Immunoblotting of cell lysates shows
696 cellular expression of HA-tagged A3F variants, relative to actin loading control Expression is
697 decreased for L306A and each double mutant, relative to HA-A3F-WT and the single α-helix
698 6 mutants (L364A, L368A, L372A). (C) Immunoblotting of virion lysates shows virion
699 incorporation of HA-tagged A3F variants, relative to HIV $p24^{Gag}$. Virion incorporation is
700 decreased for L306A and each double mutant, relative to HA-A3F-WT and the single α-helix
701 6 mutants (L364A, L368A, L372A). (D) Sucrose density gradient centrifugation followed by
702 immunoblotting using specific antibodies and chemiluminescent detection showed
703 differences in quantitative encapsidation of the single mutants. L306A (top panel) and
704 L368A (third panel) were not quantitatively encapsidated, as were L364A (second panel)
705 and L372A (fourth panel). Each panel also shows capsid ($p24^{Gag}$) in mature core
706 component-containing fractions. (E) Sucrose density gradient centrifugation followed by
707 immunoblotting using specific antibodies and chemiluminescent detection showed that
708 none of the double mutants, L306A/L368A (top panel), L364/L368A (second panel), and

709 L368A/L372A (third panel), was quantitatively encapsidated. Each panel also shows capsid
710 ($p24^{Gag}$) in mature core component-containing fractions. (F) Equal amount of viral particles
711 were used to infect TZM-bl cell to test its effect on anti-HIV-1 activity. Decreased core
712 localization diminished restriction of Vif-null HIV-1 NL4-3 by A3F. Wild-type A3F and
713 mutants with wild-type levels of cellular expression (Fig. 5B) and virion incorporation (Fig.
714 5C) are depicted as gray bars. Anti-viral activity against Vif-null HIV-1 was decreased for
715 A3F L368A (Lane 5), relative to wild-type A3F (Lane 2). L364A and L372A had activity
716 similar to wild type (Lanes 4 and 6, respectively). Since decreased virion incorporation is
717 expected to diminish restriction, variants with decreased cellular expression (Fig. 5B) and
718 virion incorporation (Fig. 5C) were compared only to each other and are shown as white
719 bars. Among the variants with similarly reduced virion incorporation (Fig. 5C), L306/L368
720 (Lane 9) had similar anti-*Vif*-null HIV activity to the other two double mutants (Lanes 7, 8)
721 and L306A (Lane 3).

722

723 **FIG. 4.** N-terminal leucine residues homologous to the C-terminal leucine residues are also
724 required for A3F core localization and anti-viral activity against Vif-null HIV-1. In these
725 experiments 10 μg of pNL4.3 Vif-null proviral clone and 1 μg of wild type or 3 μg of each
726 mutant A3F expression DNAs were used for transient transfection. After 2 days post
727 transfection cell lysates and viral supernatants were collected to test its effect on cellular
728 expression, viral incorporation, infectivity and core localization of the mutant A3Fs. (A)
729 Amino acid sequence alignment of N-and C-terminus of A3F. Leucine residues common to
730 both N- and C-termini are highlighted with boxes. (B) Immunoblotting of cell lysates shows
731 cellular expression of HA-tagged A3F variants, relative to actin loading control. Expression
732 is similar for all. (C) Immunoblotting of virion lysates shows virion incorporation of HA-

733 tagged A3F variants, relative to HIV p24^{Gag}. Virion incorporation is similar for all. (D)
734 Sucrose density gradient centrifugation and Western blotting using specific antibodies and
735 chemiluminescent detection showed differences in core localization of the single mutants.
736 L122A (top panel) and L184A (third panel) were not localized well to cores, as opposed to
737 L180A (second panel) and L188A (fourth panel). Each panel also shows capsid (p24^{Gag}) in
738 mature core component-containing fractions. (E) Equal amount of viral particles were used
739 to infect TZM-bl cell to test its effect on anti-HIV-1 activity. Anti-viral activity against Vif-null
740 HIV-1 was decreased for A3F with L122A (Row 3) and L184A (Row 5) mutants that lost
741 majority of core localization, relative to wild-type A3F (Row 1). A3F L180A (Row 4) and
742 A3F L188A (Row 6) had activity similar to wild-type A3F.

743

744 **FIGURE 5.** Double mutations into N- and C-terminal leucine residues dramatically affect
745 core localization and anti-HIV-1 activity of A3F without affecting its viral incorporation. In
746 these experiments 10 μg of pNL4.3 Vif-null proviral clone and 1 μg of wild type or 3 μg of
747 each mutant A3F expression DNAs were used for transient transfection. After 2 days post
748 transfection cell lysates and viral supernatants were collected to test its effect on cellular
749 expression, viral incorporation, infectivity and core localization of the mutant A3Fs. (A)
750 Immunoblotting analysis shows that all the A3Fs display similar cellular expression at those
751 amounts used for the transfection. GAPDH was used as a loading control (Lane 1: Vif-null
752 only, lane 2: Vif-null + WT A3F, lane 3: Vif-null + L122/L368A A3F, and lane 4: Vif-null +
753 L184/L368A A3F). (B) Immunoblotting analysis of viral pellets shows similar levels of viral
754 incorporation. As a loading control p24 was also probed (Lane 1: Vif-null only, lane 2: Vif-
755 null + WT A3F, lane 3: Vif-null + L122/L368A A3F, and lane 4: Vif-null + L184/L368A A3F).
756 (C) Core localization of A3Fs was analyzed by sucrose density gradient experiment. Unlike

757 wild-type A3F mainly localized into the core fractions, majority of double mutant A3Fs was
758 found almost exclusively outside the core fractions. (D) Equal amount of viral particles were
759 used to infect TZM-bl cell to test its effect on anti-HIV-1 activity. Both mutant A3Fs lost
760 almost all of its anti-HIV-1 activity compared to that of the wild-type protein.

Figure 1

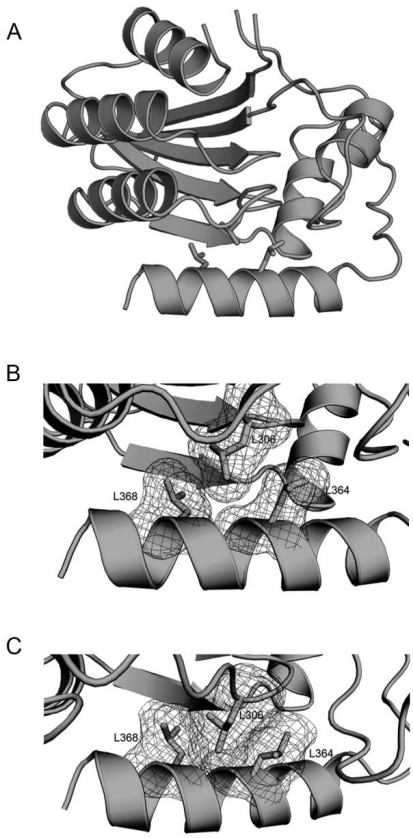

Figure 2

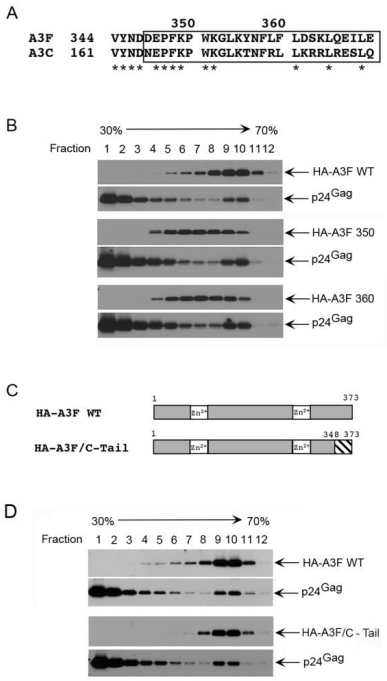

Figure 3

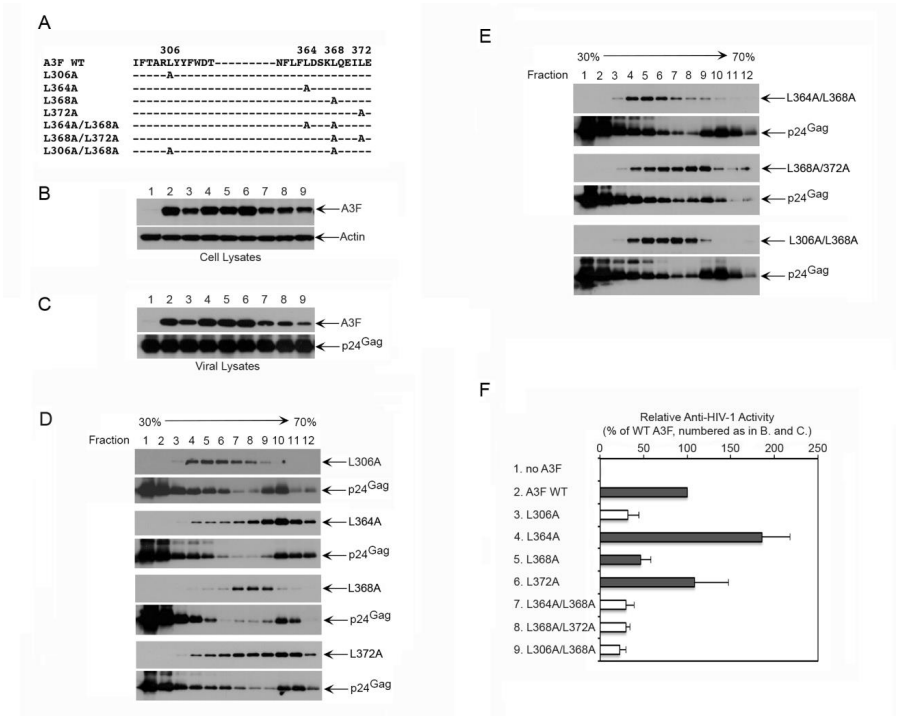

Figure 4

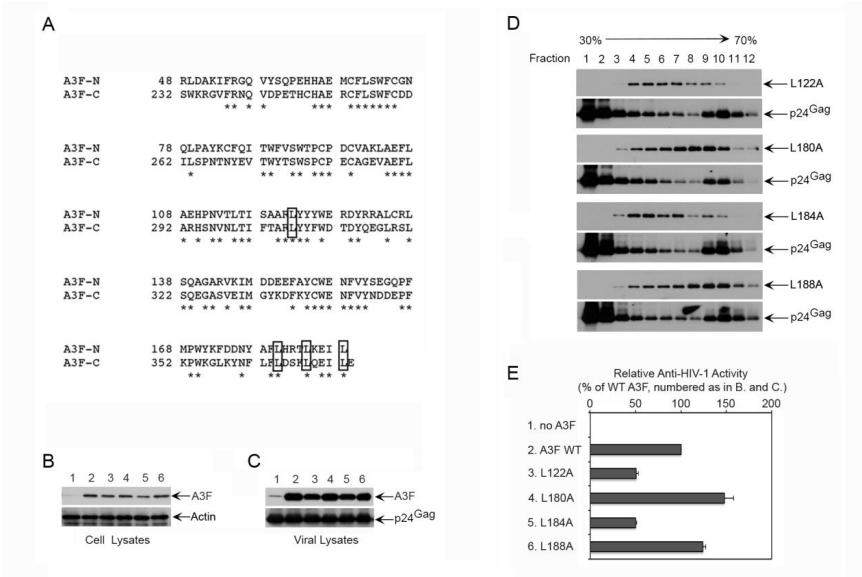

Figure 5